REPORT DOCUMENTATION PAGE

Form Approved
OMB NO. 0704-0188

1. AGENCY USE ONLY (Leave Blank)	2. REPORT DATE	3. REPORT TYPE AND DATES COVERED
	4/17/2010	Energy & Fuels 23 (2009) pp4231–4235

4. TITLE AND SUBTITLE	5. FUNDING NUMBERS
Influence of aluminum passivation on the reaction mechanism: flame propagation studies	W911NF-04-1-0217
6. AUTHOR(S)	
B. Dikici, SW Dean, ML Pantoya, VI Levitas, RJ. Jouet	
7. PERFORMING ORGANIZATION NAME(S) AND ADDRESS(ES)	8. PERFORMING ORGANIZATION REPORT NUMBER
Texas Tech University, Mechanical Engineering Department, Lubbock, TX 79409	
9. SPONSORING / MONITORING AGENCY NAME(S) AND ADDRESS(ES)	10. SPONSORING / MONITORING AGENCY REPORT NUMBER
U. S. Army Research Office P.O. Box 12211 Research Triangle Park, NC 27709-2211	

11. SUPPLEMENTARY NOTES

The views, opinions and/or findings contained in this report are those of the author(s) and should not be construed as an official Department of the Army position, policy or decision, unless so designated by other documentation.

12 a. DISTRIBUTION / AVAILABILITY STATEMENT	12 b. DISTRIBUTION CODE
Approved for public release;federal purpose rights	

13. ABSTRACT (Maximum 200 words)

Currently, two main known mechanisms of aluminum (Al) nanoparticle reaction are discussed in the literature, namely those based on diffusion through an oxide shell and melt-dispersion. The two mechanisms lead to opposite predictions in nanoparticle design. The diffusion mechanism suggests that the reduction or complete elimination of the oxide shell will increase Al reactivity, whereas the meltdispersion mechanism suggests an increase in initial oxide thickness up to an optimal value. The goal of this study is to perform critical experiments in a confined flame tube apparatus to compare these two predictions. Specifically, the flame propagation rates of perfluoroalkyl carboxylic acid (C13F27COOH)-treated Al nanoparticles with and without an alumina shell were measured. Results show that when there is no alumina passivation shell encasing the Al core, the flame rate decreases by a factor of 22-95 and peak pressure deceases by 3 orders of magnitude, in comparison with the Al particles with an oxide shell. These results imply that the melt-dispersion reaction mechanism is responsible for high flame propagation rates observed in these confined tube experiments.

14. SUBJECT TERMS	15. NUMBER OF PAGES
Reaction Mechanisms, Thermite Combustion, Aluminum Particles, Passivation of Aluminum Particles, Al synthesis techniques	5
	16. PRICE CODE

17. SECURITY CLASSIFICATION OR REPORT	18. SECURITY CLASSIFICATION ON THIS PAGE	19. SECURITY CLASSIFICATION OF ABSTRACT	20. LIMITATION OF ABSTRACT
UNCLASSIFIED	UNCLASSIFIED	UNCLASSIFIED	unclassified

NSN 7540-01-280-5500

Standard Form 298 (Rev.2-89)
Prescribed by ANSI Std. 239-18
298-102

Energy Fuels **2009,** *23,* 4231–4235 · DOI:10.1021/ef801116x
Published on Web 08/06/2009

energy&fuels
article

Influence of Aluminum Passivation on the Reaction Mechanism: Flame Propagation Studies

Birce Dikici,[†] Steven W. Dean,[†] Michelle L. Pantoya,*[,†] Valery I. Levitas,*[,‡] and R. Jason Jouet[§]

[†]*Mechanical Engineering Department, Texas Tech University, Lubbock, Texas 79409, USA,* [‡]*Department of Mechanical Engineering, Department of Aerospace Engineering, and Department of Material Science and Engineering, 2025 Black Engineering Building, Iowa State University, Ames, Iowa 50011-2161, USA, and* [§]*Research and Technology Department, Indian Head Division - Naval Surface Warfare Center, Indian Head, Maryland 20640, USA*

Received January 11, 2009. Revised Manuscript Received June 24, 2009

Currently, two main known mechanisms of aluminum (Al) nanoparticle reaction are discussed in the literature, namely those based on diffusion through an oxide shell and melt-dispersion. The two mechanisms lead to opposite predictions in nanoparticle design. The diffusion mechanism suggests that the reduction or complete elimination of the oxide shell will increase Al reactivity, whereas the melt-dispersion mechanism suggests an increase in initial oxide thickness up to an optimal value. The goal of this study is to perform critical experiments in a confined flame tube apparatus to compare these two predictions. Specifically, the flame propagation rates of perfluoroalkyl carboxylic acid ($C_{13}F_{27}COOH$)-treated Al nanoparticles with and without an alumina shell were measured. Results show that when there is no alumina passivation shell encasing the Al core, the flame rate decreases by a factor of 22−95 and peak pressure deceases by 3 orders of magnitude, in comparison with the Al particles with an oxide shell. These results imply that the melt-dispersion reaction mechanism is responsible for high flame propagation rates observed in these confined tube experiments.

Introduction

Use of nanometric ingredients offers many advantages over conventional micrometer-sized particles in the combustion of solid particle fuel and oxidizer formulations. Since nanoparticles have higher specific surface area, there are more contact points between reactants compared to micrometer-sized particles. Reduced particle size and the corresponding increased specific surface area decreases the diffusion distance between reactants and increases the homogeneity of the mixture. Greater homogeneity improves the efficiency of reaction and increases the flame speed. Therefore, reactions occur over a shorter time scale (i.e., 10 μs) compared to the micrometer particulate reactions (i.e., 10 ms).

Aumann et al.[1] examined the oxidation behavior of ultrafine grain aluminum powder using Rutherford backscattering spectrometry, thermogravimetric analysis, and high resolution transmission electron microscopy. They suggest that Al powder mixtures with 20−50 nm diameters can react 1000 times faster than micrometer particle mixtures because of the reduced diffusion distances between individual reactants.[1] Hunt et al.[2] studied the ignition and combustion behaviors of nanometric nickel and aluminum intermetallic mixtures. Laser ignition experiments on pressed Ni/Al pellets show that nanometric composites have significantly reduced ignition times over micrometer-scale composites. Granier et al. found similar results for Al and molybdenum trioxide (MoO_3).[3]

For nanoparticles, there have been many studies that examine the effect of particle size on flame speed through a mixture. One of the first investigations by Bockmon et al.[4] examined the combustion behavior of nanocomposite powder mixtures of Al and MoO_3 as a function of Al particle size. Flame speed and pressure measurements were analyzed for confined burning configurations. The average speed increased from 750 to 950 m/s when the particle size was reduced from 121 to 80 nm. Considerable changes in flame speed were not observed for mixtures with particles below 80 nm.[4]

There are currently two main mechanisms of aluminum nanoparticle oxidation applicable to the high heating rate conditions consistent with flame propagation in a tube. Each mechanism is summarized below.

Diffusion Mechanism. Conventional metallic Al fuel nanoparticles are covered by a thin (1.7−6 nm) alumina shell. During combustion the reaction is controlled by diffusion of the oxidizer and/or fuel through the growing oxide shell.[5,6] This mechanism is similar to that for micrometer particles[7,8] but also adds diffusion of aluminum toward oxygen. The diffusion mechanism was justified in ref 5 experimentally for the heating rate of 10^3 K/s. This mechanism requires at least 1 s for complete oxidation to occur, whereas the estimated

*To whom correspondence should be addressed. E-mail: michelle.pantoya@ttu.edu.

(1) Aumann, C. E.; Skofronic, G. L.; Martin, J. A. *J. of Vac. Sci. Technol., B* **1995**, *13* (3), 1178–1183.
(2) Hunt, E. M.; Plantier, K. B.; Pantoya, M. L. *Acta Mater.* **2004**, *52* (11), 3183–3191.
(3) Granier, J. J.; Pantoya, M. L. *Combust. Flame* **2004**, *138* (4), 373–383.
(4) Bockmon, B. S.; Pantoya, M. L.; Son, S. S.; Asay, B. W.; Mang, J. T. *J. Appl. Phys.* **2005**, *98* (6), 064903.
(5) Park, K.; Lee, D.; Rai, A.; Mukherjee, D.; Zachariah, M. *J. Phys. Chem. B* **2005**, *109*, 7290.
(6) Rai, A.; Park, K.; Zhou, L.; Zachariah, M. *Combust. Theory Model.* **2006**, *10*, 843.
(7) Rosenband, V. *Combust. Flame* **2004**, *137*, 366.
(8) Trunov, M. A.; Schoenitz, M.; Zhu, X.; Dreizin, E. L. *Combust. Flame* **2005**, *140*, 310.

Table 1. Material Properties of Reactant Powders[a]

material	manufacturer	particle size (nm)	oxide thickness	acid content (based on mass)	active Al (based on mass)
Al-80	NovaCentrix	80	2	71.6%	23.8%
(Al−$C_{13}F_{27}$)cd	Indian Head, NSW	100	no shell	75%	25%
(Al−$C_{13}F_{27}$)th	Indian Head, NSW	100	no shell	75%	25%
MoO3	Mach-I	44	n/a	n/a	n/a

[a] Note that $C_{13}F_{27}$ represents $C_{13}F_{27}COOH$.

reaction time in flame propagation experiments[4] is 4 orders of magnitude smaller for nanoparticles. The effect of phase transformations in the alumina shell from amorphous to crystalline phases, which leads to fracture of a shell and acceleration of oxidation, was studied in refs 9 and 10. Propagation rates for the diffusive mechanism of oxidation could be increased by reducing or completely eliminating the initial oxide shell thicknesses.

Melt-Dispersion Mechanism. Levitas et al.[11,12] propose the melt-dispersion mechanism for fast reaction of aluminum nanoparticles at fast heating rate. The melting of the Al core causes a 6% volume increase, which leads to a pressure build-up within the particle (0.1−4 GPa). This high pressure causes the oxide shell to spallate, after which the melted Al core becomes exposed and an unloading pressure wave produces large tensile pressure and disperses molten Al clusters in all directions and at high velocity. Reaction of such small bare clusters are not limited by diffusion through an oxide shell, which explains the high flame speeds experimentally observed. The melt-dispersion mechanism is schematically illustrated in ref 12.

This mechanism allows one to resolve various puzzles in Al nanoparticles combustion that cannot be explained by the diffusion mechanism. It is found in refs 11−13 that the Al particle radius, shell thickness, or aluminum content are not controlling parameters individually. Instead, there exists a relationship between Al core radius to shell thickness ratio, M, and flame speed. For $M < 19$, maximum possible flame speeds were obtained, whereas for $M > 19$ rates decreased with increasing M. In fact, an increase in shell thickness reduces M and increases flame rates, in contrast to a diffusion mechanism but in support of a melt-dispersion mechanism. Later,[14] the same relationship between flame speed and M was extended for 1−3 μm particles.

In this study, both the diffusion and melt-dispersion mechanisms are critically examined further by studying the flame speed of Al particles with and without an alumina (Al_2O_3) shell. For this reason, two types of nano-Al/metal oxide composites are examined to determine the shell's influence on flame speed. The first Al sample is passivated with Al_2O_3 and treated with perfluoroalkyl carboxylic acid ($C_{13}F_{27}COOH$). The second Al sample is devoid of an alumina shell and instead passivated with perfluoroalkyl carboxylic acid ($C_{13}F_{27}COOH$). Elimination of alumina shell should improve diffusion but make the melt-dispersion mechanism impossible. The same oxidizer (MoO_3) was used for both composites and both mixtures were prepared with similar stoichiometry . The experiments were performed to measure the pressure output and flame speed of loose powders reacting in a confined configuration.

It is noted that there are conditions under which the perfluorinated carboxylic acid-passivated Al particles exhibit improved performance over the alumina passivated Al particles. For example, in refs 15 and 16 acid-passivated Al particles combined with plastic bonded explosive (PBX) showed twice as great dent volume compared to standard Al formulations in small-scale shock reactivity and internal blasts tests. Also, in refs 16 and 17 the evolution and decay of aluminum and aluminum monoxide were monitored from laser ablation studies. Both studies show that the reaction rate of acid-passivated Al particles increased by the elimination of the oxide coating.

Experimental Section

Sample Preparation. Two different types of Al particles were studied: with and without an alumina passivation shell. The type of Al without an alumina passivation shell was further prepared using two different synthesis techniques. Physical property information for each sample is listed in Table 1. The first Al sample was purchased from NovaCentrix (formerly Nanotechnolgies) Inc., Austin, TX, with an average particle diameter of 80 nm (provided by the manufacturer who used BET). Oxide shell thickness was determined by the manufacturer. Detailed analyses of particle size distributions for particles with averaged diameter of 80 nm from NovaCentrix is presented in ref 10. These particles were then treated with the $C_{13}F_{27}COOH$ acid. This sample will be designated as Al-80.

The second type of Al sample was synthesized such that the particle has no alumina shell, but is instead passivated by perfluorotetradecanoic acid, $C_{13}F_{27}COOH$. These particles were made using two different techniques: the first was prepared from catalytic decomposition of AlH_3*N(Me)Pyr and designated as (Al−$C_{13}F_{27}$)cd; and the second was prepared from triethylaluminum thermolysis and is designated as (Al−$C_{13}F_{27}$)th. Average particle size was determined using BET. The acid content for all samples was determined based on the specific masses of Al and acid.

SEM micrographs of the composites of Al-80 with MoO_3 and (Al−$C_{13}F_{27}$)th with MoO_3 are presented in Figures 1 and 2. Figure 3 is a schematic diagram illustrating the two types of Al surface passivation examined in this study. Each type of Al particle was combined with nanoscale MoO_3, which has a rod-like morphology and was purchased from Mach-I. The active Al content for Al-80 in Table 1 refers to Al in the zero oxidation state. It is also noted that the alumina content for the Al-80 sample is 4.6% on a mass basis.

(9) Trunov, M. A.; Schoenitz, M.; Dreizin, E. L. *Combust. Theory Model.* **2006**, *10* (4), 603–623.
(10) Trunov, M. A.; Umbrajkar, S. M.; Schoenitz, M.; Mang, J. T.; Dreizin, E. L. *J. Phys. Chem. B* **2006**, *110*, 13094–13099.
(11) Levitas, V. I.; Asay, B. W.; Son, S. F.; Pantoya, M. L. *Appl. Phys. Lett.* **2006**, *89*, 071909.
(12) Levitas, V. I.; Asay, B. W.; Son, S. F.; Pantoya, M.J. *Appl. Phys.* **2007**, *101*, 083524.
(13) Levitas, V. I.; Pantoya, M. L.; Dikici, B. *Appl. Phys. Lett.* **2008**, *92*, 011921.
(14) Levitas, V. I.; Pantoya, M.; Watson, K. W. *Appl. Phys. Lett.* **2008**, *92*, 201917.
(15) Warren, A.D.; Lawrence, G.W.; Jouet, R.J. Sock Compression of Condensed Matter In *AIP Conference Proceedings*; Elert, M., Furnish, M. D., Chau, R. Holmes, N. C., Nguyen, J. Eds.; 2007; Vol *955*, pp 1018−1021.
(16) Jouet, R. J.; Carney, J. R.; Granholm, R. H.; Sandusky, H. W.; Warren, A. D. *Mat. Sci. Technol.* **2006**, *22* (4), 422–429.
(17) Jouet, R. J.; Carney, J. R.; Lightstone, J. M.; Warren, A. D. Shock Compression of Condensed Matter In *AIP Conference Proceedings*; Elert, M. Furnish, M. D., Chau, R., Holmes, N. C., Nguyen, J. Eds.; 2007; Vol *955*, pp 1247−1250.

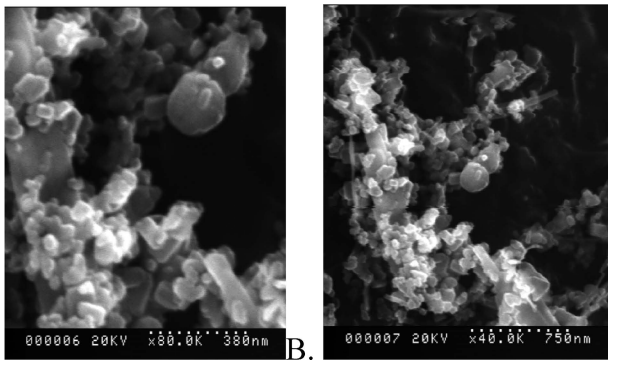

Figure 1. SEM micrographs of the postmixed composites of Al-80 with MoO_3: (A) 80 000× magnification; (B) 40 000× magnification.

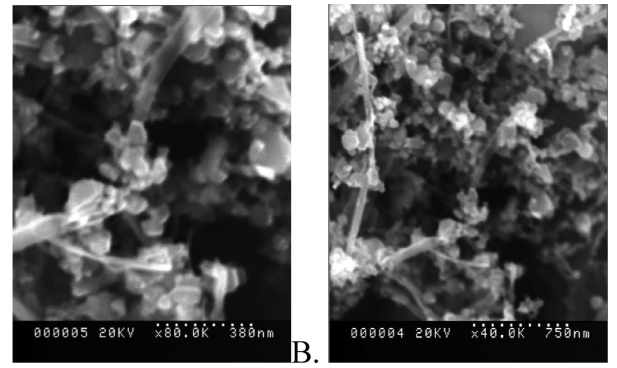

Figure 2. SEM micrographs of the postmixed composites of (Al−$C_{13}F_{27}$)th with MoO_3: (A) 80 000× magnification; (B) 40 000× magnification.

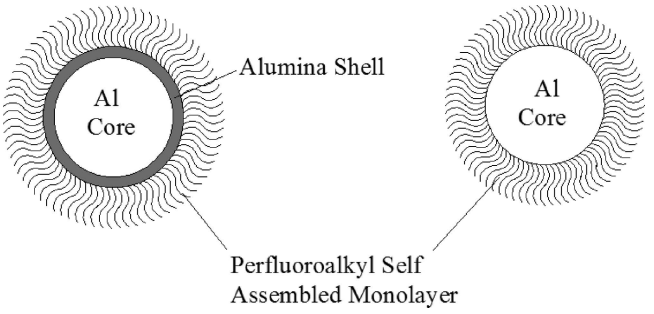

Figure 3. Schematic diagram illustrating Al surface and passivation types.

Surface passivation of Al nanoparticles by $C_{13}F_{27}COOH$ is based on a wet chemistry method. This method involves preparing and passivating the oxide-free Al.[18,19] Oxide-free Al particles can be passivated by exposure of the metal surface to $C_{13}F_{27}COOH$. This technique has been applied to several systems, but for the purposes of this paper the source of Al was the catalytic decomposition of $H_3Al \cdot N(Me)Pyr$ or thermolytic decomposition of $(CH_3CH_2)_3Al$. Passivation of the particles occurs at room temperature by exposure of the as formed Al^0 particles to a solution of $C_{13}F_{27}COOH$ in dry diethyl ether. The preparations are done under inert atmosphere and in dry solvent to prevent contamination by oxygen. The highest Al content material prepared to date contains 13 times as much

(18) Jouet, R. J.; Stern, A. G.; Rosenberg, D. M. US Patent No. US 7,192,649 B1; March 20, 2007.

(19) Jouet, R. J.; Warren, A. D.; Rosenberg, D. M.; Bellitto, V. J.; Park, K; Zachariah, M. R. *Chem. Mater.* **2005**, *17* (11), 2987–2996.

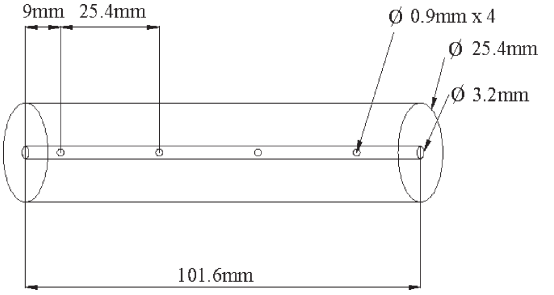

Figure 4. Schematic diagram illustrating the Acrylic tube used for flame speed measurements.

Al as $C_{13}F_{27}COOH$ on a per mole basis but is only approximately 33% Al by mass due to the high molecular weight of the acid.

A detailed description of the synthesis and characterization of Al nanoparticles without an oxide shell is presented in refs 15−18. In summary, SEM, thermogravimetric analysis (TGA) and attenuated total reflectance Fourier transform infrared spectrometry indicate that the $C_{13}F_{27}COOH$ molecule binds to the surface of the Al particle, protecting the surface from oxidation in ambient air.

For all Al particles reacting with MoO_3, it was decided not to describe the composition in terms of equivalence ratio because the competing oxidation and fluorination reactions with Al are not understood. All Al samples contain approximately the same mass percentages of Al and acid (see Table 1). The sample Al-80 also contains an additional 4.6 mass % of Al_2O_3. To each of these Al samples, a mass percent of MoO_3 was added and varied from a clearly fuel lean to fuel rich mixture. For all Al samples, the maximum flame propagation rate corresponded to 70.6 mass % MoO_3. Regardless of which oxidizer or combination thereof, this translates to a fuel rich mixture.

To combine reactants, the mixtures are suspended in hexane, and a Misonix Sonicator 3000 probe vibrating at ultrasonic speeds is used to improve mixture homogeneity. This device is programmed to produce the ultrasonic waves for 60 s with 10 s on/off intervals. This interval prevents a temperature increase and possible thermal damage to the sample. It is noted that the influence of the hexane on the reactants is not known. However, in the experiments described here, all reactants were prepared in the same way such that the effects of the mixing solution are maintained as a controlled parameter.

The mixtures are poured into a Pyrex container and placed on a hot plate at 50 °C for 10 min to evaporate the hexane. After the evaporation, the powder is reclaimed for experimentation.

Roughly 450 mg of powder mixture prepared for each mixture composition and placed into an acrylic tube shown in the Figure 4. The tube is open at both ends, and acrylic is chosen because of its transparency and strength. Transparency allows flame propagation inside the tube to be seen during combustion. More details on this apparatus can be found in ref 6.

The tubes are filled with powder, then placed onto a vibrating block and vibrated for approximately 5 s to reduce density gradients, after which more powder is added. This process results in a bulk density of 8% of the theoretical maximum density (TMD). The TMD is calculated as the ratio of the actual mass of reactants divided by sample volume to the weighted average of pure solid densities of each reactant in the matrix. In this way, a TMD of 10% describes a sample that consists of 10% solid particles and 90% air voids.

The mass in the tubes varied because of the density related with different compositions and equivalence ratios. A bent piece of Nichrome wire is placed on one side of the tube and used as the ignition source. The tube is placed into the testing block with ports for 4 PCB piezo-crystal pressure sensors used to collect

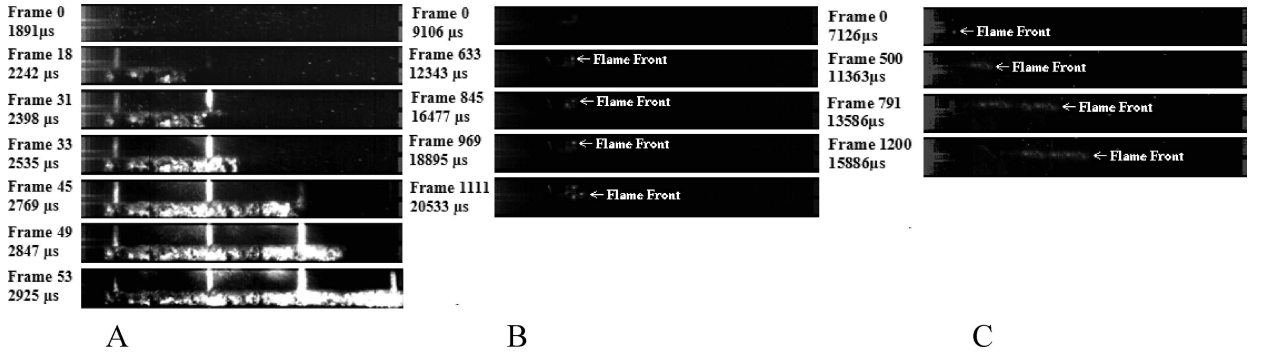

Figure 5. Consecutive frame images (A) Al-80/MoO_3; (B) (Al−$C_{13}F_{27}$)cd/MoO_3; (C) (Al−$C_{13}F_{27}$)th/MoO_3.

pressure data. The mixture is ignited at one end of the filled tube via resistance heating of the Nichrome wire.

The test block was placed in a stainless steel combustion chamber for safety purposes. The combustion chamber has an acrylic window (139.7 × 25.4 mm dimensions) that is used to obtain high-speed video of the reaction. The chamber is connected to a vacuum pump to bring the chamber to a desired pressure. A pressure gauge on the top of the chamber is used to measure the pressure. The product gases are evacuated from the chamber during and after the reaction. All experiments were performed at 1 atm in an air environment.

A Vision Research Phantom 7.1 high-speed camera was positioned perpendicular to the direction of flame propagation and was used to record flame propagation rates within the tube. The camera captures the visible emission light and takes a series of photographs at a high sampling frequency. Ignition and flame propagation were recorded at 51 000 frames per second (fps). This frame rate allowed a 16 μs temporal resolution between images. Phantom data acquisition software was used to determine the flame speed by tracking the position of the flame front with respect to time.

Pressure was measured using four PCB 113A22 piezo-crystal pressure transducers. A PCB 482A22 signal conditioner was used to convert the transducer signal into a calibrated output. A National Instruments data acquisition board was connected to the signal conditioner and controlled by Labview Version 8.0 software. Pressure data was collected at a sample rate of 100 kHz.

Results

Figure 5 show consecutive still frame images recorded at 51 000 fps. Images for mixtures of Al-80 with MoO_3 were recorded at 62 500 fps are given in ref 4.

Pressure measurements for the Al-80 and (Al−$C_{13}F_{27}$)th mixtures are given in panels A and B of Figure 6, respectively. For Al-80 mixtures the data from the fourth pressure sensor (farthest from ignition point) is used for characterizing the steady-state propagation behavior. For the (Al−$C_{13}F_{27}$)th mixtures the data from only the first pressure sensor is reported because the flame propagated only to the point between first and second pressure channels. For (Al−$C_{13}F_{27}$)cd pressure, the pressure history was not captured since the flame quenched before reaching the first pressure channel.

For the combustion of Al-80 with MoO_3, higher flame speeds (95 times higher flame speeds compared to (Al−$C_{13}F_{27}$)cd, 38 times higher flame speeds compared to (Al−$C_{13}F_{27}$)th, and 2607 times higher peak pressures compared with (Al−$C_{13}F_{27}$)th) are measured. Pressure data corresponding to both Al−$C_{13}F_{27}$ samples with MoO_3 show an insignificant pressure rise compared to Al-80 samples with MoO_3. Table 2 summarizes these results.

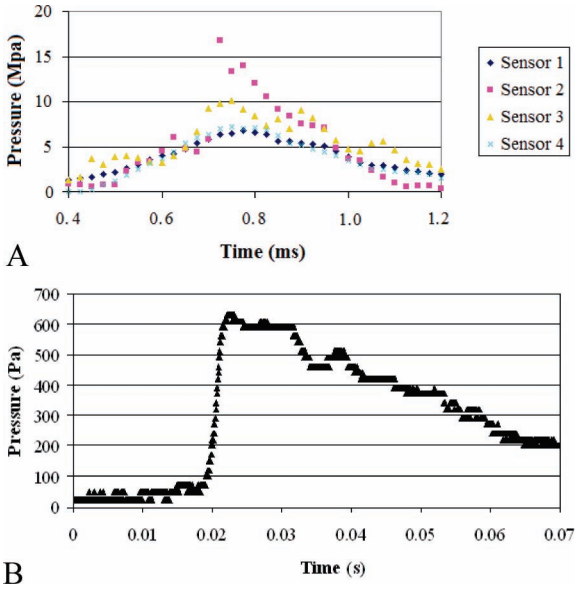

Figure 6. Pressure measurements for (A) Al-80/MoO_3 reaction and (B) (Al−$C_{13}F_{27}$)th/MoO_3.

Discussion

The results tabulated in Table 2 indicate extreme differences in flame propagation resulting from two different particle assemblies even though the chemistry of both mixtures is the same (i.e., same fuel-rich mixture composition). Promotion of diffusion and elimination of the melt-dispersion mechanism by replacing the oxide shell with a perfluoroorganic passivation layer reduced flame rate and pressure generation dramatically. This result implies that among the two alternatives, the melt-dispersion mechanism is responsible for the high flame rate of Al nanoparticles. Despite the fact that the alumina shell inhibits diffusion, does not participate in reaction (i.e., is a dead weight) and acts as a heat sink, the presence of the alumina shell is a necessary condition for the melt-dispersion mechanism that is proposed as the principle reason for the high flame propagation rates observed in reactions involving nanometric Al particles. Although these experiments do not prove directly the melt-dispersion mechanism, they are fully consistent with predictions based on this mechanism. These results are also consistent with experiments in ref 13 that show that a decrease in oxide shell thickness reduces the flame rate in experiments similar to the one presented here.

In general, flame rate depends on various parameters, including mechanism of flame propagation, Al particle size,

Table 2. Summary of Results from High-Speed Camera and Pressure Sensors for Optimal Mixture Composition[a]

reactants	Al-80	(Al−$C_{13}F_{27}$)cd	(Al−$C_{13}F_{27}$)th
mass (mg)	480	420	420
flame speed (m/s) (from high speed camera)	285.2 ± 10	3 ± 0.5	7.5 ± 0.5
peak pressure (kPa)	1676.670	N/A	0.643
rise time (μs)	228.571	N/A	682
pressurization rate (MPa/sec)	6601.89	N/A	0.10185
propagation rate (from pressure data) (m/sec)	178.6	N/A	8.13
sample rate (pps)	100 000	10 000	10 000

[a] N/A: not applicable based on quenching of the reaction.

size distribution of fuel and oxidizer particles, oxide shell thickness, the morphology of the mixture, and others. It is impossible, at least in the given case, to keep all parameters the same, excluding oxide thickness. Thus, active Al content is slightly smaller for the Al-80 sample with an oxide shell (Table 1), but this presence of alumina should reduce flame speed for them according to the traditional diffusion mechanism. The diameter of Al nanoparticles with a shell is slightly smaller than that without a shell. However, the flame speed is the same for both particle sizes if they are covered by a proper oxide shell.[13] The particle size distribution may be significantly different for samples with and without an oxide layer. However, even an addition to Al nanoparticles of up to 30% of micrometer-scale particles did not change the flame velocity.[20] For these experiments, the cleanest possible comparison was made. The point is that the difference between flame propagation rate and generated pressure for the two types of Al particles is so drastic that all these indeterminacies cannot undermine our conclusion that removing the oxide shell drastically reduces particle reactivity in the flame tube experiment. This result is not in contradiction with previous studies of the material without an oxide shell,[16−19] which show the advantages of removing the oxide shell. Indeed, for the conditions when the melt-dispersion mechanism is not operative, the diffusion reaction mechanism applies and removing the oxide shell will promote reaction.

(20) Moore, K.; Pantoya, M. L.; Son, S. F. *J. Propul. Power* **2007**, *23*, 181–187.

Conclusion

Flame propagation in a confined tube apparatus was measured for $C_{13}F_{27}COOH$-treated Al nanoparticles with and without an alumina shell. Removing the oxide shell should promote a diffusion reaction mechanism but make the melt dispersion mechanism inoperative. The alumina-passivated Al particles exhibited flame speeds on the order of 285 m/s and the acid-passivated Al particles propagated at roughly 7 m/s or was quenched. The peak pressure deceases by 3 orders of magnitude for Al particles without an oxide layer in comparison with the mixtures with Al particles that include the oxide shell. These results imply that the melt-dispersion reaction mechanism is responsible for high flame propagation rates observed in the confined tube experiments. They represent the extreme case of our previous experimental findings,[13] when the reduction in oxide shell thickness led to the reduction in flame speed, in accordance with the melt-dispersion mechanism and in contrast to the diffusion reaction mechanism. For the conditions when the melt-dispersion mechanism is not operative, reduction of the oxide shell should lead to the increase in reaction rate, according to experiments in refs 16−18.

Acknowledgment. The authors gratefully acknowledge support from the Army Research Office contract W911NF-04-1-0217 (program director Dr. Ralph Anthenien), Office of Naval Research contract N000140810104 (program director Dr. Clifford Bedford), and National Science Foundation grant CBET-0755236 (program director Dr. Phillip Westmoreland).